

Sleeping Beauty screen reveals *Pparg* activation in metastatic prostate cancer

Imran Ahmad^{a,b,1}, Ernest Mui^{a,b}, Laura Galbraith^{a,b}, Rachana Patel^{a,b}, Ee Hong Tan^{a,b}, Mark Salji^{a,b}, Alistair G. Rust^c, Peter Repiscak^{a,b}, Ann Hedley^a, Elke Markert^a, Carolyn Loveridge^{a,b}, Louise van der Weyden^c, Joanne Edwards^b, Owen J. Sansom^a, David J. Adams^c, and Hing Y. Leung^{a,b,1}

^aCancer Research UK Beatson Institute, Bearsden, Glasgow G61 1BD, United Kingdom; ^bInstitute of Cancer Sciences, University of Glasgow, Glasgow G61 1QH, United Kingdom; and ^cExperimental Cancer Genetics, Wellcome Trust Sanger Institute, Hinxton, Cambridge CB10 1SA, United Kingdom

Edited by Owen N. Witte, Howard Hughes Medical Institute, University of California, Los Angeles, CA, and approved May 17, 2016 (received for review January 28, 2016)

Prostate cancer (CaP) is the most common adult male cancer in the developed world. The paucity of biomarkers to predict prostate tumor biology makes it important to identify key pathways that confer poor prognosis and guide potential targeted therapy. Using a murine forward mutagenesis screen in a *Pten*-null background, we identified peroxisome proliferator-activated receptor gamma (*Pparg*), encoding a ligand-activated transcription factor, as a promoter of metastatic CaP through activation of lipid signaling pathways, including up-regulation of lipid synthesis enzymes [fatty acid synthase (FASN), acetyl-CoA carboxylase (ACC), ATP citrate lyase (ACLY)]. Importantly, inhibition of PPARG suppressed tumor growth in vivo, with down-regulation of the lipid synthesis program. We show that elevated levels of PPARG strongly correlate with elevation of FASN in human CaP and that high levels of PPARG/FASN and PI3K/pAKT pathway activation confer a poor prognosis. These data suggest that CaP patients could be stratified in terms of PPARG/FASN and PTEN levels to identify patients with aggressive CaP who may respond favorably to PPARG/FASN inhibition.

PTEN | PPARG | *Sleeping Beauty* | prostate cancer | metastasis

Prostate cancer (CaP) is now the most common male cancer and second leading cause of cancer mortality in the developed world (1). The majority of patients are likely to die with, rather than from, CaP, making it important to identify key pathways that confer poor prognosis, thus minimizing overtreatment.

The *PTEN* (phosphatase and tensin homolog deleted on chromosome 10) tumor suppressor gene (TSG), a key element of the PI3K pathway, is implicated in numerous human cancers (2). The PI3K pathway is altered in ~25–70% of CaP and virtually all metastatic tumors (3, 4). Homozygous *Pten* deletion in the mouse prostate leads to prostatic intraepithelial neoplasia (PIN) at 12 wk of age and invasive carcinoma after 6–9 mo (5), with the long latency suggesting additional mutations are required for disease progression. Several genes cooperate with *Pten* loss to induce tumorigenesis in mice, including either loss of tumor suppressors such as *Smad4* or *Tp53* or activation of *ErbB2* or *Erg*. However, none of these tumors fully reflect the continuum of human CaP (6–9).

Despite significant investments in clinical biobanks, next-generation sequencing, and other “omic” approaches, the heterogeneity and multifocal nature of CaP means that most of these technologies have not produced conclusive findings to inform on disease outcome, with large sample numbers and an extended follow-up required for statistical significance (4, 10). As a result, multiple genes/pathways involved in CaP have been isolated, with difficulties in identifying the “driver” events from more common background “passenger” mutations. Thus, novel approaches to induce somatic mutagenesis have been developed to identify the key genes that drive metastatic CaP in vivo. One method is to use the synthetic *Tc1/mariner* family transposon-based *Sleeping Beauty* (SB) approach (11). The SB system uses independent transgenes carrying the transposon (*T2Onc3*) and the

enzyme transposase to initiate transpositions and thus ransom somatic mutagenesis. After integration, the transposon may disrupt the expression of TSGs in neighboring sequences or over-express nearby full length/truncated oncogenes, using its promoter/splice donor site. The expression of the transposase can be ubiquitous or tissue specific (using Cre-recombinase driven by tissue specific promoters). The SB model system has been used successfully to determine low-frequency somatic mutations that are drivers of tumorigenesis (12), which is relevant in human CaP, because recent large-scale sequencing demonstrates somatic mutations are relatively rare compared with other malignancies (3).

To our knowledge, this is the first report showing acceleration of prostate tumorigenesis in a *Sleeping Beauty* system. We validate the feasibility of such a screen in a background of *Pten*^{Null}-driven CaP and demonstrate the oncogenic role of the lead candidate, namely peroxisome proliferator-activated receptor gamma (*Pparg*) in both murine and human CaP.

Results

Identification of Genes from a SB Transposon Screen on a Background of *Pten*^{Null}-Driven Prostate Cancer. *Pten*^{Null} (*PB-Cre4:Pten*^{fl/fl}) mice develop CaP after a long and variable latency, providing an opportunity to characterize genes that cooperate with *Pten* loss to promote prostate tumorigenesis. We previously demonstrated that these *Pten*^{Null} mice develop high-grade prostatic intraepithelial neoplasia (HGPIN) at 3 mo, with a slow progression to overt CaP (>10 mo), with no metastatic development up to 18 mo (6).

We hypothesized that an insertional mutagenesis approach could directly identify “driver” genes in the development of lethal CaP. Accordingly, we interbred our *Pten*^{Null} model with the *T2/Onc3* transposon SB system, with a CMV enhancer/chicken β -actin (CAG) promoter to drive transposition through epithelial-specific

Significance

Using an unbiased forward mutagenesis screen, we were able to successfully identify candidate genes that drive advanced and metastatic prostate cancer (CaP). Alterations of peroxisome proliferator-activated receptor gamma (PPARG), encoding a regulator crucial of lipid metabolism, appear to play a role in the development of metastatic CaP in both humans and mice.

Author contributions: I.A., O.J.S., D.J.A., and H.Y.L. designed research; I.A., E. Mui, L.G., R.P., E.H.T., M.S., C.L., and L.v.d.W. performed research; R.P., J.E., D.J.A., and H.Y.L. contributed new reagents/analytic tools; I.A., A.G.R., P.R., A.H., E. Markert, O.J.S., D.J.A., and H.Y.L. analyzed data; and I.A., O.J.S., D.J.A., and H.Y.L. wrote the paper.

The authors declare no conflict of interest.

This article is a PNAS Direct Submission.

Freely available online through the PNAS open access option.

¹To whom correspondence may be addressed. Email: imran.ahmad@glasgow.ac.uk or h.leung@beatson.gla.ac.uk.

This article contains supporting information online at www.pnas.org/lookup/suppl/doi:10.1073/pnas.1601571113/-DCSupplemental.

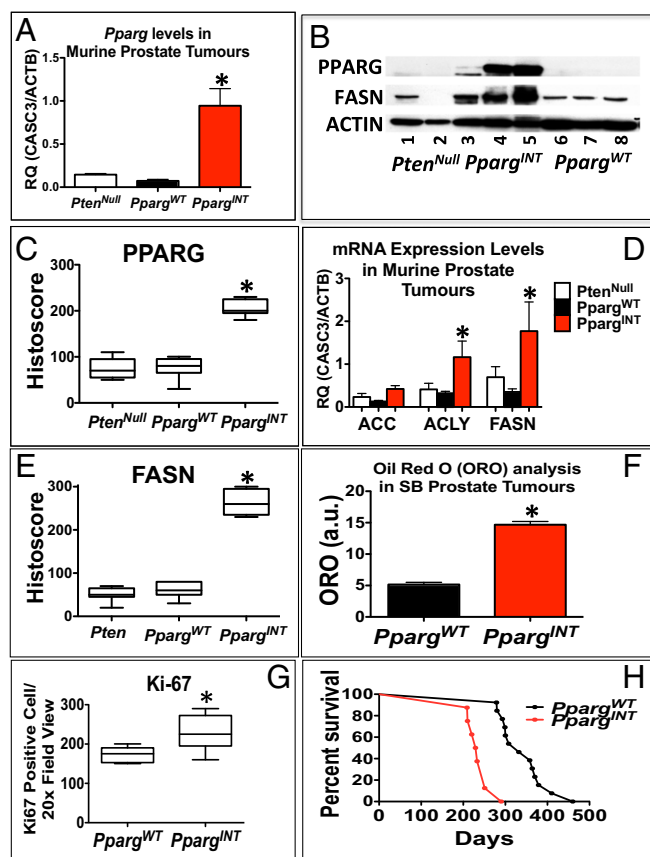


Fig. 2. Characterization of SB:*Pten*^{Null} tumors reveals oncogenic role for *Pparg*. (A) RT-PCR for *Pparg1* expression in *Pten*^{Null}, *Pparg*^{WT}, and *Pparg*^{INT} ($n = 3$, $*P < 0.0001$; Mann-Whitney). (B) Representative immunoblotting of *PPARG* and *FASN* in *Pten*^{Null}, *Pparg*^{INT}, and *Pparg*^{WT}. (C) *PPARG* and (E) *FASN* quantification of staining using histoscore in *Pten*^{Null}, *Pparg*^{WT}, and *Pparg*^{INT}, respectively, demonstrating a statistically significant increase in protein levels in *Pparg*^{INT} mice ($n = 5$, $*P < 0.005$ and $*P < 0.0001$, respectively; Mann-Whitney). (D) PCR analysis for mRNA expression of *Pparg* and genes encoding downstream lipogenic enzymes (*Acc*, *Acly*, and *Fasn*; $n = 3$, error bars represent SEM, $*P < 0.05$; Mann-Whitney). (F) Oil Red O staining quantification of triglyceride and cholesterol esters in snap frozen prostate tumors of *Pparg*^{WT} and *Pparg*^{INT} samples ($n = 3$ vs. 3, error bars represent SEM, $*P < 0.001$; Mann-Whitney). (G) Quantification of Ki-67-positive cells in *Pparg*^{INT} demonstrated increased levels of proliferation compared with *Pparg*^{WT} tumors ($n = 8$ vs. 13, $*P = 0.0008$; Mann-Whitney). (H) Kaplan-Meier (log-rank) curve demonstrating reduced survival in the *Pparg*^{INT} compared with the *Pparg*^{WT} mice ($*n = 8$ vs. 13, $P < 0.0001$).

($P = 0.0005$; Dataset S5). RNA-Seq expression data also demonstrated up-regulated expression of *Pparg* and associated genes (Table 2). Consistent with enhanced cholesterol and fatty acid biosynthesis, *Pparg*^{INT} tumors had enhanced Oil Red O staining, signifying increased levels of triglycerides and cholesterol esters (Fig. 2F; Mann-Whitney, $P < 0.001$). When we looked at the RNA-seq data, we observed that the *Pparg*^{INT} tumors had an increased basal phenotype compared with the *Pparg*^{WT} and *Pten*^{Null} tumors (Fig. S3B), in keeping with a more aggressive phenotype (15). To rule out the effect of the transposon on genes adjacent to *Pparg*, we could not demonstrate any differentially expressed genes within a 200-kb flanking region around the *Pparg* locus in those tumors with insertions at this locus (*Pparg*^{INT}) [false discover rate (FDR)-corrected Wald test, $P < 0.001$; P value represents the likelihood (less than 1 in 1,000 chance) of another differentially expressed gene being found flanking a 200-kb region on either side of *Pparg*]. As demonstrated previously (16), this suggests that transposon insertions influence the expression

of genes within close proximity to where they insert, a behavior distinct from retroviruses that can effect genes at distal sites.

When the whole cohort was analyzed, the *Pparg*^{INT} tumors demonstrated increased levels of proliferation compared with the *Pparg*^{WT} cohort ($n = 8$ vs. 13; Mann-Whitney, $P = 0.0008$; Fig. 2G). Indeed, when we looked at the survival between the cohorts, we found that the *Pparg*^{INT} subset exhibited significantly accelerated prostate tumorigenesis compared with the *Pparg*^{WT} cohort (median, 231 vs. 332 d; log-rank, $P < 0.0001$; Fig. 2H).

We next looked at *PPARG* expression in a number of human CaP cell lines (Fig. S4A). PC3 and PC3M cells (which are *PTEN* deficient) demonstrated elevated levels of *PPARG* at both the protein and mRNA level compared with the other cell lines (Fig. S4A and B). Using a highly selective and irreversible inhibitor of *PPARG*, GW9662 (17), we observed significant inhibition of proliferation (WST-1; Mann-Whitney, $P < 0.05$), colony formation (Mann-Whitney, $P < 0.0001$), and migration (in wound scratch assay) (ANOVA, $P < 0.001$) in GW9662-treated PC3 cells (Fig. S4 C–E). To further validate data from the use of GW9662, we carried out siRNA-mediated gene silencing of *PPARG* in PC3, PC3M, and DU145 cells. We confirmed that *PPARG* expression was reduced at the protein and mRNA (by >70%) level (Fig. 3A and Fig. S4 F and G). Supporting data from GW9662 treatment, siRNA knockdown of *PPARG* in PC3, PC3M, and DU145 cells significantly suppressed cell proliferation (Mann-Whitney, $P < 0.01$; Fig. 3B and Fig. S4H) and migration at 24 h (ANOVA, $P < 0.001$; Fig. 3C and Fig. S4 I and J). In addition, colony-forming assays demonstrated a reduction in the number of colonies with siRNA treatment of PC3 cells (Mann-Whitney, $P < 0.0001$; Fig. S4 K and L). We next investigated the role that down-regulation of *PPARG* activity had on its transcriptional activity using an ELISA. We found that down-regulation of *PPARG* using the GW9662 compound reduced the transcriptional activity of PC3 and PC3M cells in a statistically significant fashion (Fig. 3D).

To confirm that *PPARG* was responsible for the observed phenotype, we next transiently overexpressed *PPARG* in DU145 cells, which have low basal levels of *PPARG* (Fig. S4 A and B). This up-regulation of *PPARG* resulted in an increase in levels of *FASN* (Fig. S4M), and enhanced proliferation (Mann-Whitney, $P < 0.001$) and migration (at 18 h; ANOVA, $P < 0.01$) compared with the empty vector controls (Fig. S4 N and O).

The in vivo effects of GW9662 were tested in a PC3 orthograft model, whereby ~7 million PC3 cells were injected into the anterior prostate of individual mice. GW9662 treatment was started 2 wk later when the tumors became palpable. Mice were then culled after 4 wk of treatment. There was a trend (nonsignificant) toward inhibition of tumor growth with GW9662 treatment compared with vehicle control cohort (Fig. S5 A–C). There were, however, statistically significant reductions in Ki-67 (Fig. 3 E–G; $P < 0.0001$) and *FASN* expression (Fig. 3 H–J and Fig. S5D; $P = 0.0004$). Importantly, there was a significant reduction in the number of positive Pan-CK cells observed in the pelvic/para-aortic lymph

Table 2. Expression of selected genes related to *Pparg* insertions in the regulation of cholesterol and fatty acid metabolism

Gene symbol	<i>Pparg</i> ^{INT} vs. <i>Pparg</i> ^{WT} fold change	Adjusted P value
<i>Pparg</i>	5.378	0.0085
<i>Ppargc1b</i>	2.311	0.0403
<i>Rxra</i>	2.170	0.0106
<i>Srebf1</i>	1.620	0.0110
<i>Srebf2</i>	1.739	0.0167

Data are extracted from the RNA-Seq dataset comparing *Pparg*^{INT} vs. *Pparg*^{WT} prostate tumors (Dataset S4).

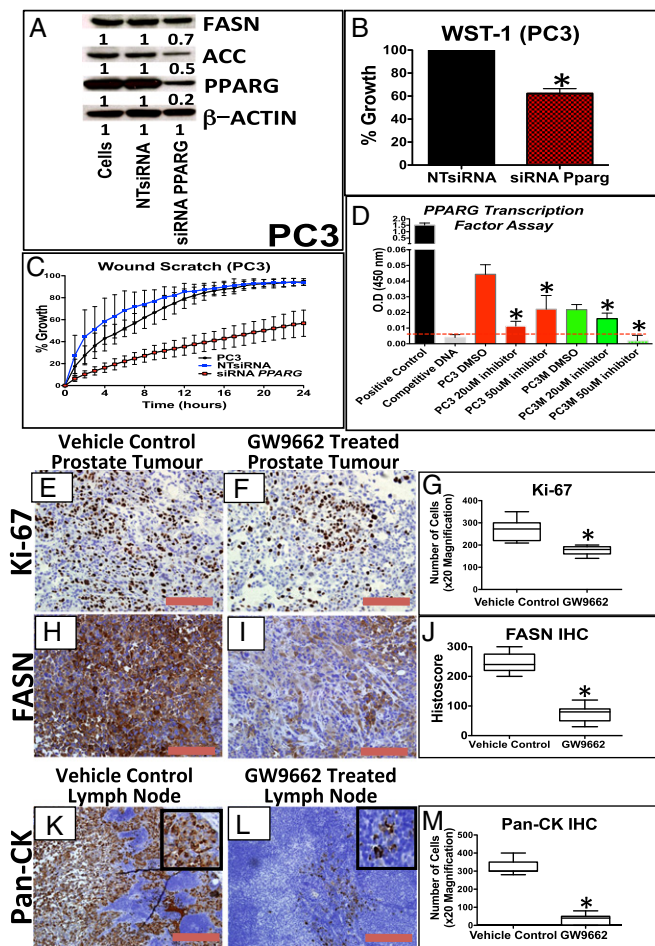


Fig. 3. Down-regulation of PPARG reduces proliferation and invasion in vitro and lymph node metastasis in an in vivo prostate orthograft model. (A) Immunoblotting for PPARG, FASN, and ACC in PC3 cells demonstrating reduction of PPARG protein expression following siRNA, along with its effects on FASN and ACC expression. (B) Following siRNA-mediated knock-down of PPARG expression (controlled with NTsiRNA), PC3 cells were functionally assessed using (B) WST-1 proliferation assay, demonstrating reduced growth ($n = 3$, error bars represent SEM, $*P < 0.01$; Mann-Whitney), and (C) wound scratch assay, demonstrating reduced migration ($n = 3$, error bars represent SD, $P < 0.001$; ANOVA). (D) ELISA-based PPARG transcription reporter assay demonstrating that GW9662 treatment (20 and 50 μM) reduced PPARG transcriptional activity in PC3 and PC3M cells compared with DMSO controls ($n = 3$, error bars represent SEM, $*P < 0.01$; Mann-Whitney). Dotted red line signifies the background signal level. (E and F) Representative IHC staining and (G) boxplot of quantification of Ki-67 staining between vehicle control and GW9662-treated PC3 orthotopic prostate tumors ($n = 6$ vs. 6, 20 \times magnification, three fields per mouse, $*P < 0.0001$; Mann-Whitney). (H and I) Representative IHC staining and (J) boxplot quantification of FASN staining between vehicle control and GW9662-treated PC3 orthotopic prostate tumors ($n = 6$ vs. 6, 20 \times magnification, three fields per mouse, $*P = 0.0004$; Mann-Whitney). (K and L) Representative IHC staining and (M) boxplot quantification Pan-CK staining in the lymph nodes between vehicle control and GW9662-treated PC3 orthograft-bearing mice ($n = 6$ vs. 6, 20 \times magnification, three fields per mouse, $*P < 0.0001$; Mann-Whitney). (Red bar, 200 μm .)

nodes of the GW9662 treated cohort, suggesting a substantial reduction in the metastatic burden ($P < 0.0001$; Fig. 3 K–M).

PPARG Expression Level Correlates with PTEN Loss and FASN Expression in Human CaP and Confers a Poor Prognosis. Using our previously published tissue microarray (TMA; $n = 229$) to investigate the expression of PPARG in CaP (6), we found that the expression of

both PPARG and FASN was up-regulated in CaP (primary Gleason grades 3–5) compared with the benign prostatic hyperplasia (BPH) control cohort (Fig. 4 A–F). In terms of co-expression, we were able to demonstrate significant correlations between up-regulated expression of PPARG with low PTEN expression (below the median; Pearson correlation coefficient, $r = 0.247$, $P < 0.0001$) and up-regulation of pAKT ($r = 0.291$, $P < 0.0001$; Table 3 and Fig. S6 A–D) (6). Interestingly, we found the

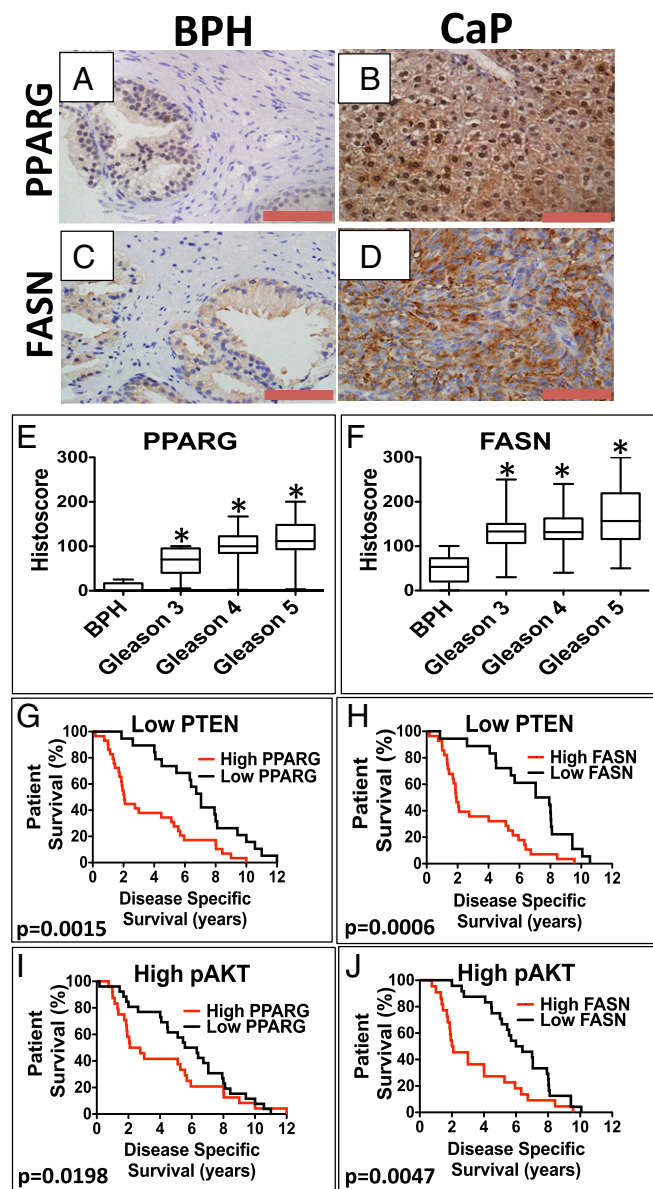


Fig. 4. Kaplan–Meier survival analysis of patients with CaP showing PPARG and FASN up-regulation along with low levels of PTEN. Representative images of IHC for (A and B) PPARG and (C and D) FASN in human BPH and CaP. (Red bar, 100 μm .) Boxplots representing histoscores of (E) PPARG and (F) FASN in BPH and primary Gleason grade 3–5 CaP. Kaplan–Meier (log-rank test) survival curves of CaP patients on a background of low PTEN levels (below the median) with (G) high expression (above median) of PPARG [compared with low (below median) PPARG; $P = 0.0015$] and (H) high expression (above median) of FASN [compared with low (below median) FASN; $P = 0.0006$]. On a background of high pAKT level (above the median), (I) high expression (above median) of PPARG [compared with low (below median) PPARG; $P = 0.0198$] and (J) high expression (above median) of FASN [compared with low (below median) FASN; $P = 0.0047$].

Table 3. Association between the expression of PPARG and PTEN/pAKT/FASN in clinical prostate cancer in our previously published TMA (n = 229) (6)

Protein expression	Pearson correlation coefficient	P value
PPARG and low PTEN	0.247	<0.0001
PPARG and pAKT	0.291	<0.0001
PPARG and FASN	0.415	<0.0001

strongest correlation between up-regulation of both PPARG and FASN levels (Pearson correlation coefficient, $r = 0.415$, $P < 0.0001$; Table 3).

Disease-specific survival (DSS) in this cohort ($n = 98/199$ patients died of CaP) demonstrated no individual association with up-regulation of PPARG, FASN, and pAKT or low PTEN status when analyzed in isolation. In addition, up-regulated PPARG or FASN on a high PTEN or low pAKT background made no difference to DSS (Fig. S6 E–H). However, patients who had up-regulated PPARG expression with low PTEN had a marked reduction in DSS compared with those patients with only low PPARG (median, 2.05 vs. 7.05 y; $P = 0.0015$; Fig. 4G). Similarly, patients with up-regulated PPARG expression with high pAKT had a reduced DSS (median, 2.09 vs. 6.32 y; $P = 0.0198$; Fig. 4I). In keeping with a functional link between PPARG and FASN, up-regulated FASN expression on both a low PTEN and high pAKT background was also associated with shorter DSS (median, 1.91 vs. 7.49 y; $P = 0.0006$, and median, 2.045 vs. 6.2 y; $P = 0.0047$, respectively; Fig. 4 H and J).

Discussion

Prostate cancer remains a significant health problem worldwide, being the most common solid organ cancer among men and second only to lung cancer as a cause of cancer-related death in males. CaP in humans is thought to arise via an accumulation of mutations in tumor related genes transforming benign prostatic epithelium to HGPIN that progresses to overt disease and subsequent metastasis. In this study, patients with CaP that have low levels of PTEN (or activation of pAKT) and accompanying PPARG (or FASN) overexpression in their prostates appear to have a poorer prognosis. In isolation, neither factor alters survival of CaP patients. In the mouse, *Pparg* activating mutations, on a background of *Pten* deletion, accelerates prostate carcinogenesis to result in metastatic disease, with associated up-regulated expression of proteins involved in lipid metabolic pathways. Importantly, treatment of a PC3 orthograft model with a PPARG inhibitor appears to negate the effects of activated PPARG, restoring the PTEN loss-induced phenotype. Additional validation could include use of a transgenic *Pten* null model that has prostate-specific *Pparg* overexpression.

A recent sequencing study of 218 CaPs found inactivating mutations in *PTEN* in 4% of primary and 42% of metastatic tumors (3). When the authors examined the entire PI3K pathway (including loss of the tumor suppressors *PHLPP* and *INPP4B*, as well as activation of the *PI3KCA* gene itself), the PI3K pathway was deregulated in 42% of primary tumors and in all metastases (3). Another recent multi-institutional sequencing study revealed somatic alteration in 49% (73/150) of the metastatic castrate-resistant prostate cancer cases (4). Therefore, within human CaP, deregulation of PI3K signaling appears essential for prostate cancer progression. Certainly in the murine context, it appears, from our data, to be vital as a “driver” mutation to instigate tumorigenesis.

PPARG is a ligand-activated transcription factor, belonging to the nuclear hormone receptor family (18). On activation by a variety of natural/synthetic PPARG agonists, heterodimerization with the retinoic acid receptor (RXR) occurs, followed by nuclear

translocation of the complex where it initiates target gene transcription through binding to the peroxisome proliferator response element (PPRE) (18). PPARG has been implicated in adipocyte differentiation, functioning as a critical link between lipid and carbohydrate metabolism (19). The role of PPARG1 (isoform 1) role in cancer biology is poorly characterized, with both tumor suppressing and oncogenic effects reported (20, 21). PPARG2 (isoform 2) is expressed at negligible levels in murine tumors and human cell lines, at both the mRNA and protein levels (18).

CaP cell lines and clinical specimens exhibit elevated levels of PPARG (22, 23). Paradoxically, it appears that PPARG activation using synthetic ligands (at high concentrations) suppresses in vitro growth in LNCaP, DU145, and PC3 prostate cancer cell lines and in vivo s.c. PC3 growth (20, 24, 25). However, recent evidence suggests these agonists may act via a PPARG-independent manner to induce cell cycle arrest and apoptosis in CaP (24).

Recent work demonstrates that loss of *Pparg* coactivator 1 α (*Pgc1 α*) is protective in chemical-induced colon and liver carcinogenesis in mice, with *Pgc1 α* activation inducing expression of a gene profile (*Acy*, *Acc*, and *Fasn*) that promotes conversion of glucose into fatty acids to support tumorigenesis (26). In our RNA-Seq data we demonstrated enrichment of *Pparg*-coactivator 1 β . It is well known that lipogenesis is a crucial factor for prostate cancer development and progression, predominantly through the enzymes *ACLY*, *ACC*, and *FASN* (27).

Our data are consistent with data on clinical CaP from cBio portal (www.cbioportal.org): *PPARG* gene amplification was found in 26% advanced CaP specimens. Interestingly, the enzyme 15-lipoxygenase-2 (*15-LOX-2*), which synthesizes 15-S-hydroxyeicosatetraenoic acid (15-S-HETE), an endogenous ligand of PPARG (28), was found up-regulated in a further 17% (Fig. S7). In total, one half of all sequenced tumors demonstrate up-regulation of one or more of the lipid synthesis genes (*FASN*, *ACC*, *ACLY*). Confirming our TMA data, if one or more of these genes is altered, there is a reduction in DSS [Memorial Sloan Kettering Cancer Centre (MSKCC) cohort; $P = 0.0181$; Fig. S7].

In summary, we demonstrate that PPARG up-regulation in a PTEN-null background will cause more aggressive tumorigenesis compared with PTEN-null tumors, with changes in expression of enzymes involved in lipid synthesis pathways. Knockdown and inhibition of PPARG appears to reduce tumorigenesis both in an in vitro and in vivo setting, whereas overexpression of *PPARG* results in a more aggressive phenotype. Collectively, our data suggest the possibility for targeted therapies using PPARG/FASN inhibitors in this CaP patient subgroup (low PTEN/high pAKT expression).

In addition, to our knowledge, we are the first to demonstrate the strength of the SB transposon model system in successfully determining low-frequency somatic mutations that may drive prostate tumorigenesis. We envisage that this type of screen could provide a useful platform to identify putative driver events in both castration- and chemotherapy-resistant CaP.

Materials and Methods

Mouse Strains. All murine experiments were approved by the Animal Welfare and Ethical Review Board (AWERB) at the University of Glasgow. Further information is given in *SI Materials and Methods*.

CIS Analysis. Information is given in *SI Materials and Methods*.

RNA Extraction. Total RNA was extracted from frozen mouse prostate tumors from *Pten*^{Null} mice and *SB:Pten*^{Null} mice with (*Pparg*^{WT}) and without (*Pparg*^{NT}) *Pparg* insertions and from human CaP cell lines using the RNeasy Mini Kit (QIAGEN; 74104) according to the manufacturer's instructions. RNA quantity and quality were evaluated by spectrophotometry using the NanoDrop 2000 spectrophotometer (Thermo Scientific) and 2100 Bioanalyzer (Agilent) RNA electropherograms, with calculation of RNA integrity number (RIN).

Quantitative Real-Time PCR. Information is provided in *SI Materials and Methods*.

Library Preparation and Sequencing. Mouse RNA samples were processed using the Illumina RNA-Seq protocol (Illumina) according to manufacturer's instructions without poly(A) mRNA selection. The libraries were prepared using the Illumina TruSeq stranded mRNA kit. Steps include poly(A) selection, fragmentation, cDNA synthesis, A tail, adapter ligation and library amplification. The amplified library was sequenced on the Nextseq 500 (Illumina) with a paired-end sequencing strategy. The read length was set at 75 nt with an expected library size of 200 bp (library size from the bioinformatic side would be the mean number of reads per sample and that is just over 61 million).

Bioinformatics. Further information is given in *SI Materials and Methods*.

IHC. IHC was performed on formalin-fixed, paraffin-embedded (FFPE) samples (details in *SI Materials and Methods*).

Microscopy. Light microscopy was carried out using the Olympus BX51.

Human TMA. We studied FFPE sections from 229 prostate cancer patients (6). Further information is given in *SI Materials and Methods*.

Immunoblotting. Western blotting was performed with the following antibodies (dilutions as per datasheets): PTEN (Cell Signaling #9559), PPAR γ (Cell Signaling #2435), FASN (Cell Signaling #3180), ACC (Cell Signaling #3676), ACLY (Cell Signaling #4332), GAPDH (Sigma #G9295), and actin (Cell Signaling #4968). Proteins were separated by SDS/PAGE and transferred by

semidry blotting onto a PVDF membrane (Immobilon-P; Millipore). Secondary HRP-linked antibodies were used in conjunction with Pierce ECL Plus Western Blotting Substrate (32132; Thermo Scientific). Further information is given in *SI Materials and Methods*.

Oil Red O Staining. Further information is given in *SI Materials and Methods*.

Cell Culture. Human prostate cancer cell lines LnCaP, CRW22, PC3, PC3M, and DU145 were authenticated by LCG standards and grown in RPMI (Gibco) containing 10% (vol/vol) serum supplement and 2 mM L-glutamine at a temperature of 37 °C with 5% (vol/vol) CO₂.

GW9662 Inhibitor Treatment. Further information is given in *SI Materials and Methods*.

Statistics. All statistical analyses (namely Mann–Whitney, Pearson correlation coefficient, ANOVA, *t* test, and Kaplan–Meier survival analysis) were performed using GraphPad Prism v5.0c. In the box whisker plots, whiskers represent minimum and maximum, and the box represents the 25th and 75th percentiles.

ACKNOWLEDGMENTS. We thank G. Kalna [Cancer Research UK (CRUK) Beatson Institute] for statistical advice, staff in the biological services unit, and the Beatson histology department. We thank C. Winchester (CRUK Beatson Institute) for useful comments in the editing of this manuscript. This work was funded by Cancer Research UK Grant C596/A17196/A15151 (to H.Y.L.) and Grant C49745/A19661 (to I.A.), and the Academy of Medical Sciences Award AMS-SGCL6-Ahmad.

- Andriole GL, et al.; PLCO Project Team (2009) Mortality results from a randomized prostate-cancer screening trial. *N Engl J Med* 360(13):1310–1319.
- Salmena L, Carracedo A, Pandolfi PP (2008) Tenets of PTEN tumor suppression. *Cell* 133(3):403–414.
- Taylor BS, et al. (2010) Integrative genomic profiling of human prostate cancer. *Cancer Cell* 18(1):11–22.
- Robinson D, et al. (2015) Integrative clinical genomics of advanced prostate cancer. *Cell* 161(5):1215–1228.
- Wang S, et al. (2003) Prostate-specific deletion of the murine Pten tumor suppressor gene leads to metastatic prostate cancer. *Cancer Cell* 4(3):209–221.
- Ahmad I, et al. (2011) HER2 overcomes PTEN (loss)-induced senescence to cause aggressive prostate cancer. *Proc Natl Acad Sci USA* 108(39):16392–16397.
- Carver BS, et al. (2009) Aberrant ERG expression cooperates with loss of PTEN to promote cancer progression in the prostate. *Nat Genet* 41(5):619–624.
- Chen Z, et al. (2005) Crucial role of p53-dependent cellular senescence in suppression of Pten-deficient tumorigenesis. *Nature* 436(7051):725–730.
- Ding Z, et al. (2011) SMAD4-dependent barrier constrains prostate cancer growth and metastatic progression. *Nature* 470(7333):269–273.
- Berger MF, et al. (2011) The genomic complexity of primary human prostate cancer. *Nature* 470(7333):214–220.
- March HN, et al. (2011) Insertional mutagenesis identifies multiple networks of co-operating genes driving intestinal tumorigenesis. *Nat Genet* 43(12):1202–1209.
- Wong CC, et al.; Chronic Myeloid Disorders Working Group of the International Cancer Genome Consortium (2014) Inactivating CUX1 mutations promote tumorigenesis. *Nat Genet* 46(1):33–38.
- Dupuy AJ, Akagi K, Largaespada DA, Copeland NG, Jenkins NA (2005) Mammalian mutagenesis using a highly mobile somatic Sleeping Beauty transposon system. *Nature* 436(7048):221–226.
- Pérez-Mancera PA, et al.; Australian Pancreatic Cancer Genome Initiative (2012) The deubiquitinase USP9X suppresses pancreatic ductal adenocarcinoma. *Nature* 486(7402):266–270.
- Smith BA, et al. (2015) A basal stem cell signature identifies aggressive prostate cancer phenotypes. *Proc Natl Acad Sci USA* 112(47):E6544–E6552.
- West AG, Fraser P (2005) Remote control of gene transcription. *Hum Mol Genet* 14(Spec No 1):R101–R111.
- Leesnitzer LM, et al. (2002) Functional consequences of cysteine modification in the ligand binding sites of peroxisome proliferator-activated receptors by GW9662. *Biochemistry* 41(21):6640–6650.
- Lehrke M, Lazar MA (2005) The many faces of PPAR γ . *Cell* 123(6):993–999.
- Celi FS, Shuldiner AR (2002) The role of peroxisome proliferator-activated receptor γ in diabetes and obesity. *Curr Diab Rep* 2(2):179–185.
- Kubota T, et al. (1998) Ligand for peroxisome proliferator-activated receptor γ (troglitazone) has potent antitumor effect against human prostate cancer both in vitro and in vivo. *Cancer Res* 58(15):3344–3352.
- Sikka S, Chen L, Sethi G, Kumar AP (2012) Targeting PPAR γ Signaling Cascade for the Prevention and Treatment of Prostate Cancer. *PPAR Res* 2012:968040.
- Subbarayan V, et al. (2004) Differential peroxisome proliferator-activated receptor- γ isoform expression and agonist effects in normal and malignant prostate cells. *Cancer Epidemiol Biomarkers Prev* 13(11 Pt 1):1710–1716.
- Segawa Y, et al. (2002) Expression of peroxisome proliferator-activated receptor (PPAR) in human prostate cancer. *Prostate* 51(2):108–116.
- Bolden A, Bernard L, Jones D, Akinyeke T, Stewart LV (2012) The PPAR γ agonist troglitazone regulates Erk 1/2 phosphorylation via a PPAR γ -independent, MEK-dependent pathway in human prostate cancer cells. *PPAR Res* 2012:929052.
- Mueller E, et al. (2000) Effects of ligand activation of peroxisome proliferator-activated receptor γ in human prostate cancer. *Proc Natl Acad Sci USA* 97(20):10990–10995.
- Bhalla K, et al. (2011) PGC1 α promotes tumor growth by inducing gene expression programs supporting lipogenesis. *Cancer Res* 71(21):6888–6898.
- Swinnen JV, et al. (2004) Androgens, lipogenesis and prostate cancer. *J Steroid Biochem Mol Biol* 92(4):273–279.
- Subbarayan V, et al. (2005) Inverse relationship between 15-lipoxygenase-2 and PPAR- γ gene expression in normal epithelia compared with tumor epithelia. *Neoplasia* 7(3):280–293.
- Wu X, et al. (2001) Generation of a prostate epithelial cell-specific Cre transgenic mouse model for tissue-specific gene ablation. *Mech Dev* 101(1-2):61–69.
- Lesche R, et al. (2002) Cre/loxP-mediated inactivation of the murine Pten tumor suppressor gene. *Genesis* 32(2):148–149.
- Dupuy AJ, et al. (2009) A modified sleeping beauty transposon system that can be used to model a wide variety of human cancers in mice. *Cancer Res* 69(20):8150–8156.
- Ahmad I, et al. (2011) Ras mutation cooperates with β -catenin activation to drive bladder tumorigenesis. *Cell Death Dis* 2:e124.
- Kirkegaard T, et al. (2006) Observer variation in immunohistochemical analysis of protein expression, time for a change? *Histopathology* 48(7):787–794.
- Taube ME, Liu XW, Fridman R, Kim HR (2006) TIMP-1 regulation of cell cycle in human breast epithelial cells via stabilization of p27(KIP1) protein. *Oncogene* 25(21):3041–3048.
- Humason GL (1972) *Animal Tissue Techniques* (Freeman, San Francisco).
- Collino M, et al. (2005) The selective PPAR γ antagonist GW9662 reverses the protection of LPS in a model of renal ischemia-reperfusion. *Kidney Int* 68(2):529–536.
- Collin M, Murch O, Thiemeermann C (2006) Peroxisome proliferator-activated receptor- γ antagonists GW9662 and T0070907 reduce the protective effects of lipopolysaccharide preconditioning against organ failure caused by endotoxemia. *Crit Care Med* 34(4):1131–1138.
- De Backer O, Elinck E, Priem E, Leybaert L, Lefebvre RA (2009) Peroxisome proliferator-activated receptor γ activation alleviates postoperative ileus in mice by inhibition of Egr-1 expression and its downstream target genes. *J Pharmacol Exp Ther* 331(2):496–503.
- Liberzon A, et al. (2011) Molecular signatures database (MSigDB) 3.0. *Bioinformatics* 27(12):1739–1740.
- Smid M, et al. (2008) Subtypes of breast cancer show preferential site of relapse. *Cancer Res* 68(9):3108–3114.
- Huper G, Marks JR (2007) Isogenic normal basal and luminal mammary epithelial isolated by a novel method show a differential response to ionizing radiation. *Cancer Res* 67(7):2990–3001.
- Subramanian A, et al. (2005) Gene set enrichment analysis: A knowledge-based approach for interpreting genome-wide expression profiles. *Proc Natl Acad Sci USA* 102(43):15545–15550.